Chin. Phys. Lett. **39**, 077301 (2022)

Spectroscopic Evidence for Electron Correlations in Epitaxial Bilayer Graphene with Interface-Reconstructed Superlattice Potentials

Chaofei Liu(刘超飞)[1] and Jian Wang(王健)[1,2,3*]

[1]*International Center for Quantum Materials, School of Physics, Peking University, Beijing 100871, China*
[2]*CAS Center for Excellence in Topological Quantum Computation, University of Chinese Academy of Sciences, Beijing 100190, China*
[3]*Beijing Academy of Quantum Information Sciences, Beijing 100193, China*

(Received 20 April 2022; accepted manuscript online 2 June 2022)

Superlattice potentials are theoretically predicted to modify the single-particle electronic structures. The resulting Coulomb-interaction-dominated low-energy physics would generate highly novel many-body phenomena. Here, by *in situ* tunneling spectroscopy, we show the signatures of superstructure-modulated correlated electron states in epitaxial bilayer graphene (BLG) on 6H-SiC(0001). As the carrier density is locally quasi-'tuned' by the superlattice potentials of a 6×6 interface reconstruction phase, the spectral-weight transfer occurs between the two broad peaks flanking the charge-neutral point. Such a detected non-rigid band shift beyond the single-particle band description implies the existence of correlation effects, probably attributed to the modified interlayer coupling in epitaxial BLG by the 6×6 reconstruction as in magic-angle BLG by the moiré potentials. Quantitative analysis suggests that the intrinsic interface reconstruction shows a high carrier tunability of $\sim$1/2 filling range, equivalent to the back gating by a voltage of $\sim$70 V in a typical gated BLG/SiO_2/Si device. The finding in interface-modulated epitaxial BLG with reconstruction phase extends the BLG platform with electron correlations beyond the magic-angle situation, and may stimulate further investigations on correlated states in graphene systems and other van der Waals materials.

DOI: 10.1088/0256-307X/39/7/077301

For twisted heterostructures between atomically thin van der Waals crystals, the electronic structures are modified by the moiré superlattice potentials via interlayer hybridization. In the two-dimensional (2D) mini Brillouin zone for moiré lattice, the continuum model of twisted bilayer graphene (BLG) predicted two low-energy bands separated by a gap.[1] Near the 'magic angle' (MA) $\theta \approx 1.05°$, the effective non-Abelian gauge potentials generated by interlayer hoppings dictate that the low-energy bands are highly non-dispersive (flat bands) near the charge-neutral point (CNP).[1−3] In such a limit of strong electron correlations, the Coulomb interaction localizes the electrons, yielding emergent many-body ground states with high gate tunability near the fractional fillings of moiré band, $\nu = 0$, $\pm\frac{1}{4}$, $\pm\frac{1}{2}$, $\pm\frac{3}{4}$, including Mott-correlated insulating states,[4−7] superconductivity,[5,6,8] ferromagnetism,[6,9] and Chern insulator.[10,11] Particularly, at half-filling, the Mott-correlated phases and derived superconductivity upon slight carrier doping show a transport phase diagram resembling the high-T_c cuprate superconductors.[4−6]

Despite the intensive literature already reported, many fundamental questions desire further explorations. (i) By integrating the scanning tunneling microscopy (STM) with the back-gate tuning of carrier doping, the signatures of electronic correlations in MA-TBG were detected behaving as distorted tunneling spectra (dI/dV vs V) when the flat band is aligned with Fermi level.[12,13] Developing a different *in situ* carrier-tuning method would be beneficial to the spectroscopic investigations of correlated physics. (ii) Signatures of correlated phase have been observed by both transport and scanning tunneling spectroscopy (STS) in BLG beyond MA of $\sim$1.05° (e.g. $\theta = 0.7°$;[14] $\theta = 0.93°$;[15] $\theta = 1.49°$[16]). In principle, twist angle and interlayer hybridization equivalently control the electronic structures of moiré crystals.[5] By tuning interlayer spacing with hydrostatic pressure (1.33 GPa), non-MA-BLG ($\theta = 1.27°$) can also show the strong insulating phase, superconductivity, and fine structures of Landau fans as unpressured MA-BLG ($\theta = 1.08°$).[5] It would be interesting to further explore the correlated states in BLG without MA.

*Corresponding author. Email: jianwangphysics@pku.edu.cn
© 2022 Chinese Physical Society and IOP Publishing Ltd

Previously, the signature of correlated phase has been detected in epitaxial pristine monolayer graphene,[17,18] which appears as the considerable deviation from the noninteracting Dirac-cone dispersion in photoemission-measured band structures. However, the electronic many-body correlations have not been reported in epitaxial bilayer graphene. Here, by *in situ* tuning the local carrier density alternatively via intrinsic interface reconstruction, we detected for the first time the STS signatures of correlated electron phase in epitaxial BLG on 6H-SiC(0001). Specifically, the 6×6 interfacial reconstruction between BLG and SiC was found to effectively modulate the spatial carrier density locally. As the Fermi energy is 'tuned' quasi-continuously, the spectral-weight transfer occurs across the CNP. Such observation deviating from the rigid band shift is beyond the noninteracting description and suggests the existence of electron correlations, which highlights the important role of interfacial 6×6 reconstruction in modifying the electronic structures of BLG.

Results—Epitaxially Grown BLG on SiC. All STM experiments were performed at 4.3 K unless specified. The BLG was synthesized in the ultrahigh-vacuum ($\sim 2\times10^{-10}$ mbar) molecular beam epitaxy (MBE) system via surface graphitization of n-type 6H-SiC(0001) by flash annealing at 1300 ℃ for 80 cycles.[19] In detail, at first, the SiC substrate is degassed at ∼650 ℃ for more than 3 h in the manipulator equipped in the MBE chamber. The flash-annealing procedure is then performed by heating the substrate from 650 to 1300 ℃ in 65 s with a steady rate of 10 ℃/s. The high temperature at 1300 ℃ is kept for 30 s. After that, the substrate is rapidly quenched to 650 ℃ in 30 s, kept for another 30 s before the next flash-annealing cycle. The whole procedure, including temperature variation and cycling, is code-controlled. The substrate temperature was measured with an infrared thermometer. Typically, the graphitized SiC shows step heights of 0.75 nm [Fig. 1(a)]. Essentially, the triple bilayer-SiC (0.25 nm ×3) steps uniformly capped by BLG naturally result in the 0.75-nm-high steps.[19,20] The primarily obtained epitaxial BLG is Bernal-stacked [Fig. 1(d)] with a triangular atomic lattice [Fig. 1(b)]. Fast-Fourier-transformation (FFT) analysis [upper inset of Fig. 1(b)] yields the lattice constant $a_0 \approx 0.26$ nm, comparable with $a_0 = 0.246$ nm for pristine graphene.

Tunneling spectra were acquired by the standard lock-in technique[21] [for schematic of STM apparatus, see Fig. 1(c)]. Distinctive gap- and dip-like anomalies are revealed at Fermi energy E_F and [−500, −400] mV, respectively [lower inset of Fig. 1(b)]. The gap is attributed to the absence of phonon-mediated inelastic tunneling within $\pm\Omega$ (Ω, phonon threshold energy),[22] whereas the dip that appears as a local differential-conductance minimum is indicative of the Dirac-type CNP nominally at eV_D.[22] The Fermi level shifted by 400–500 meV above eV_D is well comparable to previously reported epitaxial graphene/SiC,[17,23,24] suggesting the highly electron-doped nature of the epitaxial BLG. In essence, the E_F shift is attributed to the doping of graphene layer by the depletion of surface electrons at interface between the buffer layer and n-type SiC.[25] The interlayer coupling in Bernal-stacked BLG breaks the A/B sublattice symmetry of individual graphene layers. The resulting electronic structures are gapped with parabolic dispersions, yielding massive Dirac fermions.[26] This contrasts the linear dispersion of massless Dirac carriers in monolayer graphene, and explains the nonlinear local density of states (LDOS) in the BLG spectrum near the CNP [lower inset of Fig. 1(b)].

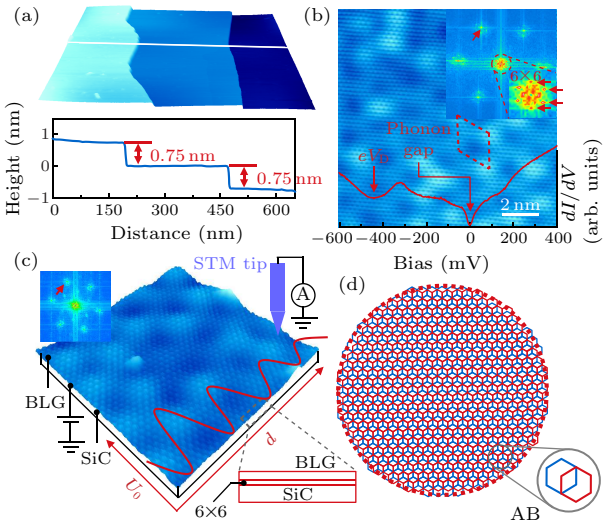

Fig. 1. Epitaxial BLG on 6H-SiC(0001). (a) Upper: large-scale topographic image of graphitized SiC (size: 650×650 nm^2; set point: $V = 1$ V, $I = 500$ pA); lower: linecut profile along the white line in upper panel. (b) Topographic image of the epitaxial BLG on SiC (size: 12×12 nm^2; set point: $V = 0.4$ V, $I = 500$ pA), showing the triangular atomic lattice accompanied by 6×6 reconstruction phase (supercell indicated as dashed diamond). Upper inset: FFT of the main panel, where the Bragg point for atomic lattice is indicated by a tilted arrow, and the 6×6 features are zoomed in and highlighted by horizontal arrows. Lower inset: typical tunneling spectrum; the 'phonon' gap (see main text) at E_F and the CNP eV_D at local differential-conductance minimum are highlighted [set point: $V = 0.04$ V, $I = 500$ pA; modulation: $V_{mod} = 6$ mV (by default unless specified)]. (c) Schematic of the STM setup, integrated with the small-scale topography of BLG (size: 5×5 nm^2; set point: $V = 0.4$ V, $I = 500$ pA). Upper inset: FFT of the main panel. Lower inset: schematic profile of BLG/SiC with the interface 6×6 reconstruction. U_0, electrostatic potential; d, distance. (d) Bernal (AB) stacking of the BLG on SiC.

Interface-Modulated Spatial Electron Density. Note that a reconstruction pattern exists in BLG periodically [Fig. 1(b)], which follows the morphology of the C-rich 6×6 interface reconstruction beneath BLG with respect to the surface unit cell of SiC(0001) ($a_0 \approx 0.307\,\mathrm{nm}$) [lower inset of Fig. 1(c)].[27,28] The existence of 6×6 reconstruction pattern is further supported by the corresponding low-momentum hexagonal spots in the FFT image of BLG topography [marked by 6×6, upper inset of Fig. 1(b)]. In the flash-annealing procedure for SiC graphitization, the 6×6 superstructure develops at the initial stage of graphene formation, serving as the buffer layer for graphene epitaxy. Compared with graphene, the 6×6 reconstruction buffer layer has the same honeycomb-type network of sp^2-derived σ bands, but without the graphene-like π bands responsible for the relativistic Dirac fermions.[29] Theoretically, the local topography curvature can induce spatially varying electrochemical potential.[30] In addition, in a twisted moiré superlattice, the LDOS is modulated in space with the same period as the moiré pattern.[31] Following these spirits, despite the negligible interaction between BLG and SiC,[32] the 6×6 interface reconstruction phase would similarly generate effective periodic potential field in BLG and locally modulate the LDOS. Given that the 6×6 reconstruction arises from the periodic C–Si bonding strength,[33] the spatially modulated LDOS is essentially an intrinsic effect for the graphene epitaxially grown on SiC.

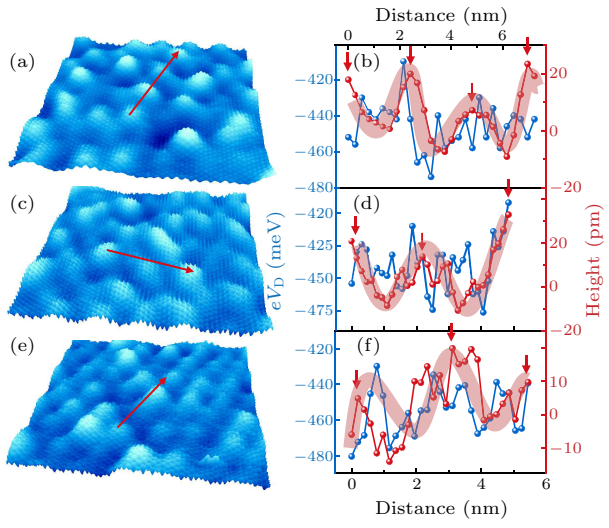

Fig. 2. Nominal CNP energy modulated by the 6×6 reconstruction phase. [(a), (c), (e)] Topographic images of BLG in different positions with size $12.5 \times 12.5\,\mathrm{nm}^2$; set point: (a) $V = 0.3\,\mathrm{V}$, $I = 500\,\mathrm{pA}$, (b) $V = 0.35\,\mathrm{V}$, $I = 500\,\mathrm{pA}$, (c) $V = 0.4\,\mathrm{V}$, $I = 500\,\mathrm{pA}$. [(b), (d), (f)] Spatial dependences of eV_D and height along the arrows in (a), (c), and (e), respectively. The short arrows mark the approximate positions of the local height maxima. The shadowed wide strips are guides to the eyes of variations of eV_D and height.

In our experiments, along different trajectories across the 6×6-reconstructed topographic 'humps', eV_D and the LDOS-dominated 'height' *roughly* change synchronously (Fig. 2). For quantitative analysis, the data points of eV_D are plotted against height, showing a statistical trend towards their positive correlation overall (Fig. S1 in the Supplementary Material). In STM configurations, $I(V) \propto e^{-\frac{2}{\hbar}\sqrt{2m\varphi}\Delta d} \int_{-eV}^{0} d\varepsilon \rho_\mathrm{s}(\varepsilon + eV)$ (φ, tunneling potential barrier; Δd, tip–sample distance; ρ_s, sample LDOS), meaning that the STM topographic image carries the information of integrated sample LDOS, $\int_{-eV}^{0} d\varepsilon \rho_\mathrm{s}(\varepsilon + eV)$, besides measuring the topographic fluctuations $\Delta d(x, y)$. From the $I(V)$ formula, we can see that, for atomically flat sample surface, which is the situation of our epitaxial BLG, the integrated sample LDOS reflected in the measured STM topographic image is nonnegligible, because the linear dependence of $I(V)$ on integrated sample LDOS prevails over the exponential dependence of $I(V)$ on Δd when $\Delta d(x, y)$ remains approximately constant. Based on these arguments, as in the moiré superlattice, the observed periodic STM topographic fluctuations in BLG induced by 6×6 reconstruction phase are mainly attributed to the potential-field-modulated LDOS of BLG [cf. Fig. 1(c)]. Accordingly, the LDOS would locally modulate the electron density n, and thus, effectively modulate the Fermi level E_F and the nominal CNP energy eV_D, consistently explaining the 'height'-tuned eV_D as observed. These 'entangled' eV_D and height profiles establish the pronounced charge-density modulation intimately controlled by the 6×6 interface reconstruction. Notably, the eV_D and height profiles are superimposed by random fluctuations [Figs. 2(b), 2(d), and 2(f)]. This can be a result of the additional doping from donor-like states in the buffer layer and its interface with SiC substrate.[34]

Electron Correlations Revealed by Spectral-Weight Transfer. The interface-reconstructed non-gated BLG behaves equivalently as a periodic array of spatially doping-evolving back-gated 'mini-devices'. The CNP eV_D extracted from STS has been commonly used as a local measure of the charge density because of its charge sensitivity.[22] Preliminarily, for typical tunneling spectra with different eV_D (i.e., different dopings), we found that the spectral intensities flanking eV_D appear mutually complementary [Fig. 3(a)]. More specifically, as eV_D increases approaching E_F [light → dark red curve in Fig. 3(a)], the intensity of the lower band (LB) below eV_D roughly increases. Meanwhile, the intensity of the upper band (UB) right above eV_D decreases accordingly. Since the 6×6-superlattice-potential-tuned LDOS can modulate eV_D via modulating the electron density n, as shown in Fig. 3(b), by

re-ordering the locally measured tunneling spectra by increasing eV_D, the electron density can be regarded as being effectively tuned quasi-continuously. On the whole, the complementary effect can be seen for the spectral intensities flanking eV_D.

Purely according to the false-color plot [Fig. 3(b)], the evolutionary trend of LB and UB appears relatively weak. To quantify the spectral intensities of LB and UB for quantitatively describing the complementary effect, the tunneling spectra were tentatively fitted by a multi-Gaussian function (Fig. S2). The spectral weights of the Gaussian components for LB and UB were extracted separately by integral as W_{LB} and W_{UB} [Fig. 3(c)]. Figure 3(d) plots W_{LB} and W_{UB} as functions of eV_D. Evidently, W_{LB} and W_{UB} show positive and negative correlations with eV_D, respectively, consistent with the qualitative judgment based on Fig. 3(b). These phenomena are highly reproducible for several different sets of spatially resolved tunneling spectra (Fig. S3). The contrast of eV_D dependences for W_{LB} and W_{UB} directly suggests the local-charge-variation-tuned spectral-weight transfer between LB and UB [Fig. 3(e)].

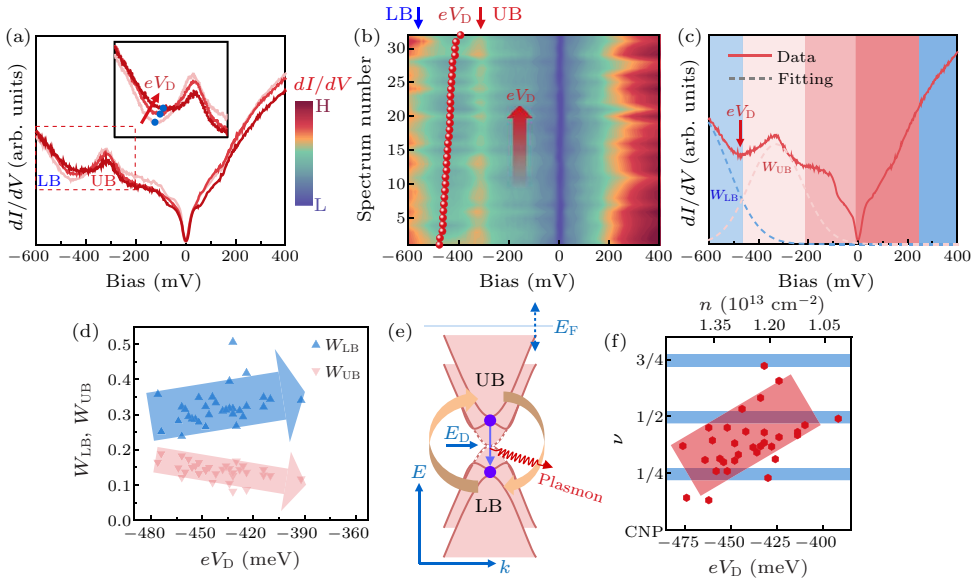

Fig. 3. Spectral-weight transfer in BLG. (a) Tunneling spectra at several typical eV_D extracted from spectra collected at different positions. Inset: zoom-in view of the spectra within the dashed rectangle for more clearly showing the spectral evolution as eV_D (blue dots) changes. The arrow highlights the eV_D-increasing direction among different spectra. (b) False-color plot of the tunneling spectra taken along the arrow in Fig. 2(c), but *ordered based on increasing* eV_D (instead of spatial position) as indicated by the thick arrow. (c) Gaussian components (dashed curves) for LB and UB flanking the CNP obtained from the multi-Gaussian fit to the tunneling spectrum. The integrated spectral weights are denoted as W_{LB} and W_{UB}, respectively (for all components involved in the multi-Gaussian fit, see Fig. S2). (d) Normalized spectral weights W_{LB} and W_{UB} extracted from the spectra in (b) plotted vs eV_D. (e) Schematic of the spectral-weight transfer between LB and UB, and plasmon emission for states near CNP. (f) eV_D dependence of the filling factor ν within LB calculated from (d) as described in the main text.

Previously, in a back-gated MA-BLG ($\theta = 1.07°$) device, the spectral-weight transfer induced by gate tuning was attributed to a signature of Mott-type correlations.[35] In pristine Bernal-stacked BLG, signatures of spectral-weight transfer across the CNP have similarly shown up by the macroscopic carrier tuning via gate voltage,[36] although further analysis is absent. In the weak-coupling mean-field picture, tuning the Fermi energy via carrier doping purely results in the rigid band shift in the single-particle electronic structures, where the kinetic energy U_t at Fermi energy E_F is larger than the Coulomb interaction U. The detected spectral-weight transfer is beyond the noninteracting, single-particle description, and essentially can be attributed to the electron-correlation effects. Note that while the neutrality point eV_D increases as local carrier tunning, UB and LB do not shift in energy following eV_D. Such non-rigid band-shift behavior beyond single-particle scenario can be consistently incorporated within the correlation explanation. A thorough theoretical description of the observations remains lacking. In phenomenology, the interface-modulated spectral-weight transfer here is reminiscent of the doping-induced spectral-weight redistribution between Hubbard band and charge-transfer gap in a doped Mott insulator.[37,38] Such resemblance implies the Mott-like correlated phase as a candidate explanation (part SI). Indeed, high-resolution ARPES for BLG on 6H-SiC reveals a flat-band dispersion at $\bar{K}$ point.[39] More concretely, the detected electron-correlation effect can be induced by the plasmarons derived from the electron–plasmon coupling for the

electronic states near Dirac point, as previously established in pristine quasi-free-standing graphene on SiC by photoemission spectroscopy [Fig. 3(e); part SII].[17,18]

High Carrier Tunability of 6×6 *Interfacial Reconstruction Phase.* For the back-gated MA-BLG ($\theta = 1.07°$), a gate voltage of $\Delta V_g \approx \pm 15\,\mathrm{V}$ shows a carrier-tuning ability of half-filling $\Delta\nu = \pm\frac{1}{2}n_s$ ($n_s = 4/A_0 = 2.7 \times 10^{12}\,\mathrm{cm}^{-2}$, i.e. four carriers per moiré supercell A_0) of the fourfold spin–valley degenerate flat band.[35] Note that the degree of spectral-weight transfer therein provides a sensitive measure of the local charge. Semi-quantitatively, the local filling fraction ν can be estimated from the spectral weights of LB and UB, i.e., $\nu = 2(\frac{W_{LB}}{W_{LB}+W_{UB}} - \frac{1}{2})$.[35] For epitaxial BLG, ν ('pseudo-filling') within LB below E_F was similarly defined purely for quantifying the carrier tunability of 6×6 reconstruction. Figure 3(f) presents the extracted ν plotted vs eV_D. Profoundly, the intrinsically available electron density modulated by the 6×6 reconstruction can access a filling range of $\nu = \frac{1}{8}n_s'$–$\frac{5}{8}n_s'$ (n_s', 'full filling' of LB). This highlights a striking carrier-tuning ability of the interface reconstruction highly comparable with the gating technique.

By excluding the inelastic-tunneling effect involving the acoustic phonon $\Omega \approx 27\,\mathrm{meV}$ (defined as half the 'phonon'-gap energy), the true CNP energy E_D in graphene band structures should be modified according to $|E_D| = e|V_D| - \Omega$.[22] Further referring to the n–E_D relation for ideal graphene, $n(\boldsymbol{r}) = \frac{E_D^2(\boldsymbol{r})}{\pi(\hbar v_F)^2}$, we converted eV_D to the local carrier density n (assuming Fermi velocity $v_F = 10^6\,\mathrm{m/s}$) [Fig. 3(f)]. The estimated n falls within 9.8×10^{12}–$1.5 \times 10^{13}\,\mathrm{cm}^{-2}$, corresponding to a strikingly high doping range of $\Delta n = 5.2 \times 10^{12}\,\mathrm{cm}^{-2}$ ($= 1.9n_s$ as in MA-BLG). In the gate-tunable BLG/SiO_2/Si device, based on a simple parallel-plate capacitor model, the carrier density n directly scales with applied gate voltage V_g as $\Delta n = \alpha\Delta V_g$. Here, α is determined by the gate capacitance, $\alpha = \frac{\varepsilon_0\varepsilon}{te}$ (ε_0 and ε, permittivities of free space and SiO_2, respectively; t, thickness of SiO_2), and concretely, $\alpha = 7.19 \times 10^{10}\,\mathrm{cm}^{-2}\cdot\mathrm{V}^{-1}$ for 300-nm SiO_2.[36] Based on these discussions, the electron-density range Δn for BLG/SiC here corresponds to $\Delta V_g = 72.3\,\mathrm{V}$, indeed comparable with the measured $\Delta V_g = 55$–$85\,\mathrm{V}$ for tuning $\Delta n = 2n_s$ in BN/SiO_2-back-gated MA-BLG devices.[12,35] Therefore, the local charge modulation by 6×6 interface reconstruction can be physically equivalent to the back gating by a high voltage of $\sim 70\,\mathrm{V}$ in a typical BLG/SiO_2/Si device.

Discussions. In atomically thin 2D van der Waals heterostructures, the interlayer-hybridized moiré superlattice and the large effective mass of electrons are two crucial ingredients in the engineered Mott-correlated phase. For BLG/SiC, while the effective mass is unknown, the moiré-equivalent interlayer hybridization by the 6×6 interface reconstruction in BLG remains predominately workable. Recall that in the hydrostatic-pressured non-MA-BLG ($\theta = 1.27°$) with tuned interlayer coupling, the correlated insulating state was observed 'unexpectedly' at half-filling, where superconductivity is induced by further hole doping.[5] The filling sequence of Landau level in this pressured non-MA-BLG is identical to that in Bernal-stacked BLG. From these perspectives, the observation of electron correlations in Bernal BLG can be presumably expected, as indeed suggested previously by the observation of flat-band dispersion therein[39] via the nonlocal technique, e.g., ARPES. This highlights the importance of 6×6 interface superlattice potentials in modifying the interlayer hybridization. For decisive check over the role of the 6×6 reconstruction, control experiment may be recommended via intercalating H atoms between buffer layer and SiC to saturate the interface C–Si bonds for removing the 6×6 buffer phase.[40]

The following difference between the detected electron-correlation effects in epitaxial BLG and MA-BLG may be noted. (i) The electronic structures are modified by the interlayer hybridization tuned by the moiré superlattice in MA-BLG, but tuned by the 6×6 superstructure in epitaxial BLG. (ii) In MA-BLG, the electron correlations are revealed as the *whole* carrier density is continuously tuned by the gate voltage (e.g. into the fractional-filling regime), ranging from hole- to electron-doped region. However, in epitaxial BLG, the correlation effect is captured as the *local* carrier density is tuned quasi-continuously by the 6×6 reconstruction, all within electron-doped region. (iii) The correlated electronic states attributed to the Mott physics normally occur near E_F for MA-BLG. However, the correlated electrons are observed near the CNP far below E_F here, as the situation for the correlated electrons with plasmon emissions observed in the epitaxial monolayer graphene/SiC.[17,18] From this angle, the correlations revealed by weight transfer most probably arise from the electron–plasmon coupling specifically.

The detected charge modulation may also be affected by the local fluctuations of the in-built dipole field created across the BLG layers. During the sublimation process for preparing BLG, the interface between BLG and 6H-SiC(0001) crystal can become chemically inhomogeneous. Note that BLG epitaxially grown on SiC has a dipole field induced between the SiC depletion layer and the charge-accumulated

graphene layer next to the interface. The chemically inhomogeneous interface would produce local changes in the surface dipole. This in turn would modulate the CNP, which further blurs the statistical relation between 6×6 superstructure and $eV_{\rm D}$ [Figs. 2(b), 2(d) and 2(f)] to a broadened scatter diagram (Fig. S1), and leads to the fluctuations seen in dI/dV spectra ordered by $eV_{\rm D}$ [Fig. 3(b)].

Perspectives. Our results by STM/STS suggest that the previously overlooked many-body correlations are required to describe the electronic properties of interface-modulated Bernal-stacked BLG. The observation extends the correlated BLG system beyond MA limitation, relaxing the requirement of precise angle controlling in twisted BLG. Different from the situation in moiré superlattice with a twisted MA, where the correlated-insulator state and the superconductivity are mutually verified in transport T–n diagram, the correlated phase in our experiments is visualized locally by the spectroscopic technique. Considering that the electrical transport involves the carriers within $k_{\rm B}T$ of $E_{\rm F}$, for sufficiently high charge density $[(E_{\rm F}-E_{\rm D})>k_{\rm B}T]$ in our situation, the observed electron correlations will hardly affect the equilibrium transport properties. However, if the low-doping limit $[k_{\rm B}T>(E_{\rm F}-E_{\rm D})]$ can be realized, correlated carriers near the CNP would participate in transport. In consequence, the finding may stimulate explorations for additionally tracing the doping evolution towards the correlation-derived superconducting state at an atomic scale and establishing a more direct connection to high-$T_{\rm c}$ cuprates beyond the purely phenomenological similarity in transport phase diagrams. In the future, the suppression of dipole fluctuations during growth process and the elaborate high-resolution STS data are highly desired to further clarify the interface reconstruction modulation and the corresponding electron correlations.

Acknowledgments. This work was supported by the National Natural Science Foundation of China (Grant Nos. 11888101 and 11774008), the National Key R&D Program of China (Grant Nos. 2018YFA0305604 and 2017YFA0303302), the Beijing Natural Science Foundation (Grant No. Z180010), and the Strategic Priority Research Program of Chinese Academy of Sciences (Grant No. XDB28000000).

References

[1] Bistritzer R and MacDonald A H 2011 *Proc. Natl. Acad. Sci. USA* **108** 12233
[2] Trambly de Laissardière G, Mayou D and Magaud L 2010 *Nano Lett.* **10** 804
[3] Suárez M E, Correa J D, Vargas P, Pacheco M and Barticevic Z 2010 *Phys. Rev. B* **82** 121407
[4] Cao Y, Fatemi V, Demir A, Fang S, Tomarken S L, Luo J Y, Sanchez-Yamagishi J D, Watanabe K, Taniguchi T, Kaxiras E, Ashoori R C and Jarillo-Herrero P 2018 *Nature* **556** 80
[5] Yankowitz M, Chen S, Polshyn H, Zhang Y, Watanabe K, Taniguchi T, Graf D, Young A F and Dean C R 2019 *Science* **363** 1059
[6] Lu X, Stepanov P, Yang W, Xie M, Aamir M A, Das I, Urgell C, Watanabe K, Taniguchi T, Zhang G, Bachtold A, MacDonald A H and Efetov D K 2019 *Nature* **574** 653
[7] Polshyn H, Yankowitz M, Chen S, Zhang Y, Watanabe K, Taniguchi T, Dean C R and Young A F 2019 *Nat. Phys.* **15** 1011
[8] Cao Y, Fatemi V, Fang S, Watanabe K, Taniguchi T, Kaxiras E and Jarillo-Herrero P 2018 *Nature* **556** 43
[9] Sharpe A L, Fox E J, Barnard A W, Finney J, Watanabe K, Taniguchi T, Kastner M A and Goldhaber-Gordon D 2019 *Science* **365** 605
[10] Serlin M, Tschirhart C, Polshyn H, Zhang Y, Zhu J, Watanabe K, Taniguchi T, Balents L and Young A 2020 *Science* **367** 900
[11] Shen C, Ying J, Liu L, Liu J, Li N, Wang S, Tang J, Zhao Y, Chu Y and Watanabe K 2021 *Chin. Phys. Lett.* **38** 047301
[12] Xie Y, Lian B, Jack B, Liu X, Chiu C L, Watanabe K, Taniguchi T, Bernevig B A and Yazdani A 2019 *Nature* **572** 101
[13] Choi Y, Kemmer J, Peng Y, Thomson A, Arora H, Polski R, Zhang Y, Ren H, Alicea J, Refael G, von Oppen F, Watanabe K, Taniguchi T and Nadj-Perge S 2019 *Nat. Phys.* **15** 1174
[14] Kima K, DaSilvab A, Huangc S, Fallahazada B, Larentisa S, Taniguchid T, Kenji W B J L, MacDonaldb A H and Tutuca E 2017 *Proc. Natl. Acad. Sci. USA* **114** 3364
[15] Codecido E, Wang Q, Koester R, Che S, Tian H, Lv R, Tran S, Watanabe K, Taniguchi T, Zhang F, Bockrath M and Lau C N 2019 *Sci. Adv.* **5** eaaw9770
[16] Ren Y N, Lu C, Zhang Y, Li S Y, Liu Y W, Yan C, Guo Z H, Liu C C, Yang F and He L 2020 *ACS Nano* **14** 13081
[17] Bostwick A, Ohta T, Seyller T, Horn K and Rotenberg E 2007 *Nat. Phys.* **3** 36
[18] Bostwick A, Speck F, Seyller T, Horn K, Polini M, Asgari R, MacDonald A H and Rotenberg E 2010 *Science* **328** 999
[19] Wang Q, Zhang W, Wang L, He K, Ma X and Xue Q 2013 *J. Phys. Condens. Matter* **25** 095002
[20] Hupalo M, Conrad E H and Tringides M C 2009 *Phys. Rev. B* **80** 041401
[21] Liu C, Wang G and Wang J 2019 *J. Phys.: Condens. Matter* **31** 285002
[22] Zhang Y, Brar V W, Wang F, Girit C, Yayon Y, Panlasigui M, Zettl A and Crommie M F 2008 *Nat. Phys.* **4** 627
[23] Brar V W, Zhang Y, Yayon Y, Ohta T, McChesney J L, Bostwick A, Rotenberg E, Horn K and Crommie M F 2007 *Appl. Phys. Lett.* **91** 122102
[24] Zhou S Y, Gweon G H, Fedorov A V, First P N, de Heer W A, Lee D H, Guinea F, Castro N A H and Lanzara A 2007 *Nat. Mater.* **6** 770
[25] Berger C, Song Z, Li T, Li X, Ogbazghi A Y, Feng R, Dai Z, Marchenkov A N, Conrad E H and First P N 2004 *J. Phys. Chem. B* **108** 19912
[26] McCann E and Fal'ko V I 2006 *Phys. Rev. Lett.* **96** 086805
[27] Owman F and Mårtensson P 1996 *J. Vac. Sci. Technol.* **14** 933
[28] Chen W, Xu H, Liu L, Gao X, Qi D, Peng G, Tan S C, Feng Y, Loh K P and Wee A T S 2005 *Surf. Sci.* **596** 176
[29] Emtsev K V, Seyller T, Speck F, Ley L, Stojanov P, Riley J D and Leckey R C G 2007 *Mater. Sci. Forum* **556** 525
[30] Kim E A and Neto A C 2008 *Europhys. Lett.* **84** 57007
[31] Yankowitz M, Xue J, Cormode D, Sanchez-Yamagishi J D,

Watanabe K, Taniguchi T, Jarillo-Herrero P, Jacquod P and LeRoy B J 2012 *Nat. Phys.* **8** 382
[32] Seyller T, Emtsev K V, Speck F, Gao K Y and Ley L 2006 *Appl. Phys. Lett.* **88** 242103
[33] Kim S, Ihm J, Choi H J and Son Y W 2008 *Phys. Rev. Lett.* **100** 176802
[34] Ristein J, Mammadov S and Seyller T 2012 *Phys. Rev. Lett.* **108** 246104
[35] Jiang Y, Lai X, Watanabe K, Taniguchi T, Haule K, Mao J and Andrei E Y 2019 *Nature* **573** 91
[36] Rutter G M, Jung S, Klimov N N, Newell D B, Zhitenev N B and Stroscio J A 2011 *Nat. Phys.* **7** 649
[37] Eskes H, Meinders M B and Sawatzky G A 1991 *Phys. Rev. Lett.* **67** 1035
[38] Cai P, Ruan W, Peng Y, Ye C, Li X, Hao Z, Zhou X, Lee D H and Wang Y 2016 *Nat. Phys.* **12** 1047
[39] Marchenko D, Evtushinsky D, Golias E, Varykhalov A, Seyller T and Rader O 2018 *Sci. Adv.* **4** eaau0059
[40] Riedl C, Coletti C, Iwasaki T, Zakharov A A and Starke U 2009 *Phys. Rev. Lett.* **103** 246804

Supplementary Material for

Spectroscopic evidence for electron correlations in epitaxial bilayer graphene with interface-reconstructed superlattice potentials

Chaofei Liu(刘超飞)[1] and Jian Wang(王健)[1,2,3,*]

[1] International Center for Quantum Materials, School of Physics, Peking University, Beijing 100871, China
[2] CAS Center for Excellence in Topological Quantum Computation, University of Chinese Academy of Sciences, Beijing 100190, China
[3] Beijing Academy of Quantum Information Sciences, Beijing 100193, China

[*]E-mail: jianwangphysics@pku.edu.cn

SUPPLEMENTARY TEXT

I. Discussion About Mott Correlated Phase as the Candidate Origin of Detected Spectral-Weight Transfer

In the Mott–Hubbard model for *d*-electron systems, the interplay of on-site Coulomb energy U, kinetic energy U_t, bandwidth W, and filling factor v cooperatively drives the Mott-insulator transition [1]. The strong electron correlations are set by the high ratio of the on-site Coulomb interaction U to the bandwidth W of the flat band. In the Mott–Hubbard scenario, the strong on-site Coulomb repulsion forbids neighboring electron hopping; further at half-filling, Mott insulator occurs as the ground state with a correlated charge gap between the 'splitted' upper and lower Hubbard bands derived from the *d*-electron band [1].

Experimentally, in the doped Mott phase of cuprates, as increasing the doping level, the spectral weight transfers from Hubbard bands to charge-transfer gap near E_F as in-gap excitations [2,3]. These excitation modes 'straddle' the simultaneously formed sharp V-shaped gap at E_F. With further carrier doping towards the underdoped superconducting (SC) regime, the V-shaped gap can finally evolve into the SC gap [3]. The resemblance between our result and such spectral-weight transfer in a doped Mott insulator indicates the Mott correlation as a likely explanation.

In the candidate Mott picture for our BLG, the Dirac-type conductance dip, where the CNP is located and where the LB/UB overlap, should be a correlated gap separating the Hubbard bands by U in essence. Physically, the relative spectral weights of LB and UB flanking the correlated gap sensitively depend on the local carrier density, naturally reconciling the observed spectral-weight transfer behavior [Fig. 3(d)].

II. Electron Correlations Arising from Electron–Plasmon Coupling

We now discuss the possible concrete mechanism responsible for the detected electron correlations. Theoretically, plasmarons have been proposed in 2D electron gas defined as the resonantly coupled electron–plasmon composite excitations [4]. In the spectral function $A(\boldsymbol{k},E)$ and the LDOS spectra, the signal of the plasmaron appears as a satellite peak aside from the most tightly bounded conventional quasiparticle peak (main peak) [4,5]. By increasing chemical doping and/or disorder, the plamaron signature is expected to be suppressed [4,5].

For graphene, previous study shows that the carrier decaying via plasmon scattering is a well-defined quasiparticle only outside the region of kinematically allowed electron–hole excitations in $(E,\boldsymbol{k})$ phase diagram [6]. This constraint causes that the states near Dirac point interact strongly with the plasmons [Fig. 3(d)], meaning that the plasmarons can have a large influence on the many-body effect around $E\sim E_D$ [6,7]. Consistently, in experiments by angle-resolved photoemission spectroscopy (ARPES), the lower-energy plasmaron satellite band and the higher-energy main band straddling the Dirac point far below E_F (~−0.5 eV) have been detected in the spectral function of quasi-free-standing graphene, where the plasmaron band appears suppressed by higher chemical doping [8]. Furthermore, while the interactions between quasiparticles and plasmons are stronger in the 2D massless Dirac system than in an ordinary 2D parabolic-band system [7], the plasmaron in a 2D massive-electron system (e.g. GaAs quantum well) is still observed by tunneling spectroscopy [9]. All these arguments suggest that, the LB near Dirac energy in our BLG, which behaves as the satellite band of UB and is suppressed as increasing electron doping (more negative eV_D) [Figs. 3(a)–3(c)], can be

interpreted as the plamaron band. Equivalently speaking, the electron correlations probably arise because of the plasmon emissions for electrons near the Dirac point [Fig. 3(d)], i.e., the plasmarons consisting of resonantly bounded electrons and plasmons.

Compared with the plasmaron peak in quasi-free-standing graphene directly grown epitaxially on SiC [8], the plasmaron band in ordinary epitaxial graphene on buffer layer/SiC is normally not well resolvable in the ARPES-measured spectral function due to the high dielectric screening (with effective dielectric constant ε 3–4 times higher), which is likely further damped by the disorder in the sample. Thus, the spectral-weight transfer indicated by STS provides an alternative method to effectively reveal the many-body effect induced by the electron–plasmon coupling in ordinary epitaxial graphene.

Note that the plasmon emission occurs for the states near E_D [6]. The gap opening at E_D for epitaxial BLG would weaken the plasmaron response. Furthermore, the plasmaron band usually occurs at an energy roughly proportional to E_F or carrier density [8,10]. Yet, the energies of LB and UB here appear approximately unchanged with doping as shifting E_F (such absence of rigid following for LB and UB is also an indication of the existence of electron correlations) [Fig. 3(a)], which is left for future explorations for a full understanding within the plasmaron scenario.

SUPPLEMENTARY FIGURES

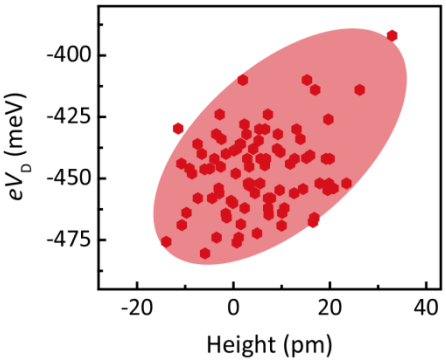

FIG. S1. Statistical correlation between eV_D and height. The data point are extracted from Figs. 2(b), 2(d) and 2(f), appearing positively correlated more clearly in statistics. The shaded ellipse is the guide to the eyes of the statistical positive correlations between eV_D and height.

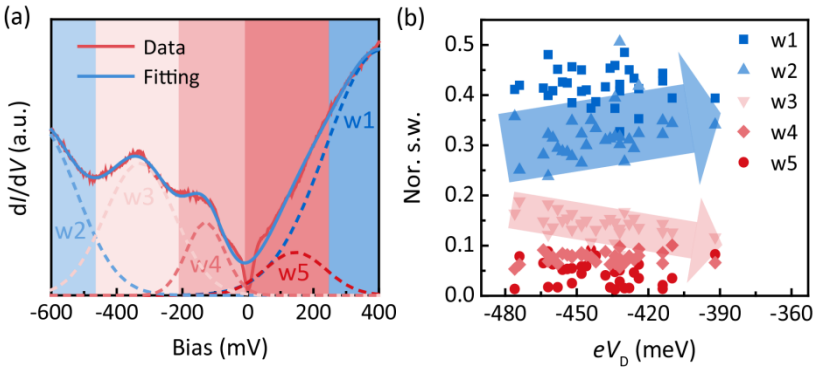

FIG. S2. Full information of the multi-Gaussian fit. (a) Exemplifying multi-Gaussian fit (solid blue curve) to the tunneling spectrum (solid red curve). The 'phonon' gap is ignored in the fit procedure. The involved five Gaussian components with integrated spectral weights w1–w5 are shown in dashed curves. Note that w2 (w3) is equal to w_{LB} (w_{UB}) as defined in main text. (c) Normalized spectral weights (s.w.) w1–w5 extracted from the spectra in (a) plotted vs. eV_D. Clearly, while w2 and w3 show positive and negative correlations with eV_D, respectively, w1, w4, and w5 behave eV_D-independent statistically, highlighting the truly existent spectral-weight transfer between w2 and w3.

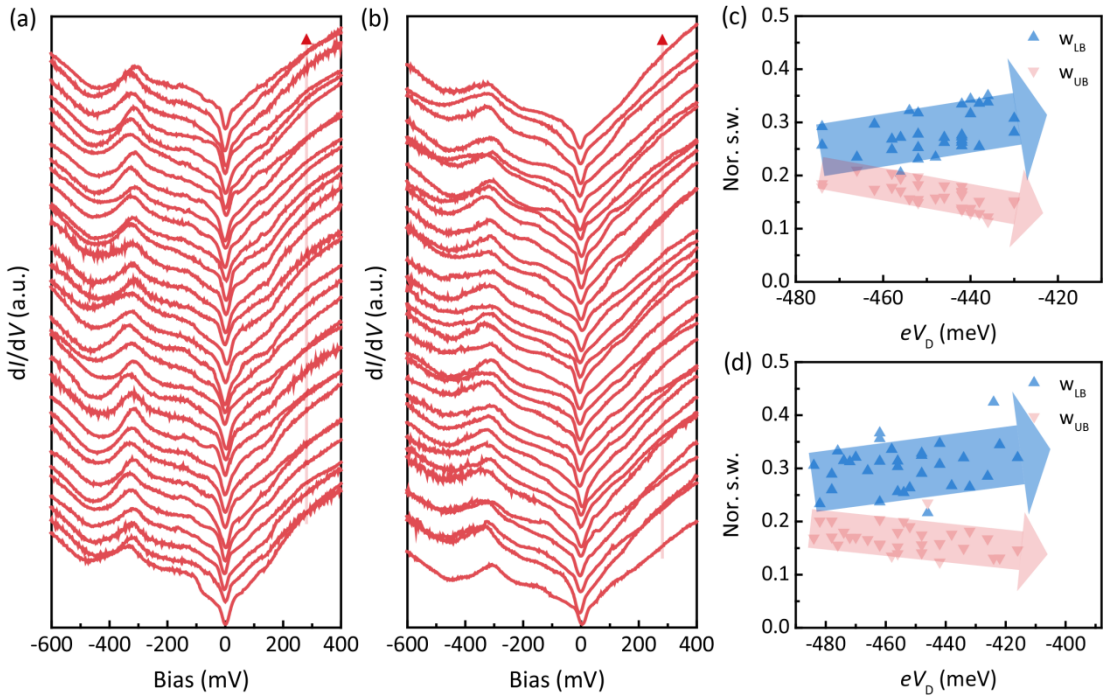

FIG. S3. Reproducibility of the spectral-weight transfer in BLG. (a,b) Tunneling spectra (vertically offset for clarity) taken along the arrows in Figs. 2(a) and 2(e), respectively. (c,d) Normalized spectral weights w_{LB} and w_{UB} extracted from the spectra in (a,b), respectively, plotted vs. eV_D.

REFERENCES

[1] Imada M, Fujimori A and Tokura Y, 1998 Metal-insulator transitions Rev. Mod. Phys. **70,** 1039.

[2] Eskes H, Meinders M B and Sawatzky G A, 1991 Anomalous transfer of spectral weight in doped strongly correlated systems Phys. Rev. Lett. **67,** 1035.

[3] Cai P, Ruan W, Peng Y, Ye C, Li X, Hao Z, Zhou X, Lee D-H and Wang Y, 2016 Visualizing the evolution from the Mott insulator to a charge-ordered insulator in lightly doped cuprates Nat. Phys. **12,** 1047.

[4] Jalabert R and Das Sarma S, 1989 Many-polaron interaction effects in two dimensions Phys. Rev. B **39,** 5542.

[5] von Allmen P, 1992 Plasmaron excitation and band renormalization in a two-dimensional electron gas Phys. Rev. B **46,** 13345.

[6] Bostwick A, Ohta T, Seyller T, Horn K and Rotenberg E, 2007 Quasiparticle dynamics in graphene Nat. Phys. **3,** 36.

[7] Polini M, Asgari R, Borghi G, Barlas Y, Pereg-Barnea T and MacDonald A H, 2008 Plasmons and the spectral function of graphene Phys. Rev. B **77,** 081411.

[8] Bostwick A, Speck F, Seyller T, Horn K, Polini M, Asgari R, MacDonald A H and Rotenberg E, 2010 Observation of plasmarons in quasi-freestanding doped graphene Science **328,** 999.

[9] Dial O, Ashoori R, Pfeiffer L and West K, 2012 Observations of plasmarons in a two-dimensional system: Tunneling measurements using time-domain capacitance spectroscopy Phys. Rev. B **85,** 081306.

[10] Dial O E, 2007 Single Particle Spectrum of the Two Dimensional Electron Gas thesis, Massachusetts Institute of Technology, Cambridge, MA.